Testing the ρ_* scaling of thermal transport models: predicted and measured temperatures in the Tokamak Fusion Test Reactor dimensionless scaling experiments

D. R. Mikkelsen, S. D. Scott
Princeton Plasma Physics Laboratory
P.O. Box 451, Princeton, NJ 08543

W. Dorland
Institute for Fusion Studies
University of Texas, Austin, TX 78712

Abstract

Theoretical predictions of ion and electron thermal diffusivities are tested by comparing calculated and measured temperatures in low (L) mode plasmas from the Tokamak Fusion Test Reactor [D. J. Grove and D. M. Meade, Nucl. Fusion **25**, 1167 (1985)] nondimensional scaling experiments. The DIII-D [J. L. Luxon and L. G. Davis, Fusion Technol. **8**, 441 (1985)] L-mode ρ_* scalings, the transport models of Rebut-Lallia-Watkins (RLW), Boucher's modification of RLW, and the Institute for Fusion Studies-Princeton Plasma Physics Laboratory (IFS-PPPL) model for transport due to ion temperature gradient modes are tested. The predictions use the measured densities in order to include the effects of density profile shape variations on the transport models. The uncertainties in the measured and predicted temperatures are discussed. The predictions based on the DIII-D scalings are within the measurement uncertainties. All the theoretical models predict a more favorable ρ_* dependence for the ion temperatures than is seen. Preliminary estimates indicate that sheared flow stabilization is important for some discharges, and that inclusion of its effects may bring the predictions of the IFS-PPPL model into agreement with the experiments.

PACS categories: 52.25.Fi, 52.55.Dy, 52.55.Fa, 52.65.-y

I. INTRODUCTION

Dimensionless scaling experiments are expected to reveal the physically significant parametric dependences of plasma transport. The dependence on ρ_* , in particular, is needed to extrapolate [1] from current experiments to International Tokamak Experimental Reactor [2] (ITER) class tokamaks. This paper compares the predictions of several experimental ρ_* scalings and theoretical transport models to the results of the Tokamak Fusion Test Reactor [3] (TFTR) dimensionless scaling experiments [4].

The dimensionless scaling experiments on several tokamaks grew out of a generic theoretical framework which has been refined over a number of years [5–8]. Within this framework theoretical diffusivities are expressed as

$$\chi = \chi_{\rm B} F\left(\rho_*, p_1, p_2, ..., p_n\right),$$

where the dimensionless variables include a normalized gyroradius, ρ_*, and several other dimensionless parameters, p_i, which are relevant to the theory at hand.

The ρ_* dependence is particularly important for extrapolating [1] from existing tokamaks to larger, hotter ignited tokamaks such as ITER5 Both the Joint European Torus [9] (JET) and the DIII-D [10] tokamak can produce plasmas with dimensionless parameters similar to ignited ITER plasmas with the exception that ρ_* is larger in the present experiments. If the transport scaling with respect to this single parameter were understood then we could more confidently predict the parameters which are needed for an ignited tokamak.

It is generally expected that the dependence of F on the small parameter ρ_* is a power law. Many theories based on short wavelength turbulence have a particular dependence which has come to be called gyro-reduced Bohm, or gyroBohm, scaling:

$$\chi = \chi_{\rm B} \rho_* F_2(p_1, p_2, ..., p_n).$$

Likewise, the absence of ρ_* dependence is referred to as Bohm scaling, and $\chi \propto {\rho_*}^{-1/2}$ is known as super-Bohm or Goldston scaling since it follows from a global scaling typical of the low (L) mode,

$$\tau_{\rm E} \propto I_{\rm p} {\overline{n}_{\rm e}}^0 {B_{\rm tor}}^0 P_{\rm heat}^{-1/2}.$$

Single fluid analyses of the local transport in L-mode tokamak discharges have found both gyroBohm and Bohm scaling. In DIII-D gyro-Bohm scaling was seen with electron cyclotron heating (ECH) in low density plasmas, while Bohm scaling was seen with ECH in higher density plasmas [11] and with neutral beam injection (NBI) in high-q plasmas [12]. Bohm scaling was seen in JET with ion cyclotron heating [13], and in TFTR with NBI [4].

A deeper understanding of the DIII-D results has emerged from two-fluid analyses of the electrons and ions separately [12]. The disparate single fluid results have been reconciled by the recognition of differing ρ_* dependences for the electron and ion thermal diffusivities in L-mode discharges: the electron diffusivity exhibits gyroBohm scaling while the ions are Goldston-like. The single fluid scaling depends on the relative importance of the two channels in a particular regime: in low density rf heated plasmas where the electron channel is dominant the single fluid local diffusivity would tend to be gyroBohm, while in neutral beam heated plasmas the ions tend to dominate and the Bohm-like overall scaling results from a mix of the different underlying scalings of the ions and electrons.

This unifying rule for L-mode discharges has an exception: a low-q L-mode ρ_* scaling experiment in DIII-D [14] which has Bohm-like scaling of $\chi_{\rm i}$ rather than the Goldston scaling seen in other L-mode experiments (but $\chi_{\rm e}$ remained gyroBohm). Furthermore, the ion diffusivity scaling is gyroBohm or Bohm-like in DIII-D H-mode discharges. A more general understanding which will connect these results is actively being sought. This work may be advanced by considering whether the mixed scalings described above are consistent with the ρ_* scalings in JET and TFTR, and by correlating the conditions under which agreement is or is not found.

It is unclear whether the L-mode ρ_* results in JET [13] are consistent with the DIII-D findings. These experiments used ion cyclotron radio frequency heating exclusively (to maintain a constant deposition profile), which tends to heat electrons preferentially. One might expect the single-fluid

analysis to follow the gyroBohm electron scaling, but in high density rf heated experiments in DIII-D the ion-electron coupling was strong enough to cause the single fluid scaling to be Bohm-like. Resolution of the issue requires a full two-fluid analysis which includes the ion-electron coupling, but this is precluded by the lack of ion temperature data for these discharges.

Both T_e and T_i were measured in the TFTR nondimensional scaling experiments so we can test the DIII-D scalings. We use a hybrid predictive method: the inferred χ_i and χ_e from one shot are scaled to the conditions of other shots and used to predict the temperatures, which are compared to the actual T_e and T_i. The predictions of another 'naive' scaling (depending only on ρ_*) with gyroBohm χ_e and χ_i are compared with the predictions of theoretical transport models.

We report predictions of the Rebut-Lallia-Watkins model [15], a modification of RLW by Boucher [16], and a critical gradient model derived from simulations of ion temperature gradient (ITG) driven turbulence [17]. In the first and last of these models both the electron and ion diffusivities have gyroBohm scalings (as is the case for many theoretical models [8]). The inadequacy of the ion diffusivity in the RLW model was partially rectified by Boucher's modified Bohm-like χ_i [16].

In ρ_* scaling experiments the other nondimensional parameters are not held strictly constant, and Waltz [18] has pointed out that these variations may change the transport sufficiently to mask the underlying ρ_* dependence. Near marginal stability an apparently small change in some parameters (e.g., the density gradient) may have a large effect on the diffusivity. As a consequence, either gyroBohm or Bohm models could be used to successfully simulate [18] the DIII-D NBI experiments which showed a Bohm scaling for the single fluid effective diffusivity. Similarly, imperfections near the plasma edge in ρ_* scaling experiments on DIII-D, JET, and TFTR strongly affect simulations based on a gyroBohm transport model [19,20]. The simulations agree with the measurements, but none of the experiments exhibit overall gyroBohm scaling. In the simulations reported here the measured density profiles and the measured temperatures at the boundary location are used in order to include any effects on transport caused by any imperfect scaling of these quantities. In this way the theories are fairly tested even though the experiments are imperfect.

Following a discussion of the TFTR nondimensional scaling experiments we describe the hybrid prediction method. The predicted temperatures are compared to the measurements, and the relevant uncertainties are discussed. Finally, the results are summarized and topics for further study are briefly discussed.

II. TFTR NONDIMENSIONAL SCALING EXPERIMENTS

The TFTR nondimensional scaling experiments [4] produced multi-shot scans of neutral beam heated L-mode discharges. The present work deals with the two scans of ρ_*, which are referred to as the low- and high-density scans. In several of the discharges the electron and ion temperatures were insufficiently decoupled to permit meaningful analysis of the electron thermal diffusivity. As a consequence, a single-fluid analysis of the local power flows was used to determine the scalings [4]. The power flows in both ρ_* scans were best represented by Bohm scaling. Foreshadowing the results presented below, the power flow scaling was not well represented by the RLW model.

The input data for this study are the output of the transport analysis codes TRANSP [21–23] and SNAP [24]: the plasma profiles (such as electron density) mapped from major to minor radius, the heating and particle source profiles (calculated by simulations of neutral beam injection and fast ion thermalization, etc.), and the inferred thermal diffusivities obtained by solving the power balance equations. Our predictions based on the experimental DIII-D scalings use the inferred χ_i and χ_e from one shot scaled to the conditions of other shots to predict the temperatures (see IV.A below).

The principal difference between the two codes is that SNAP assumes the plasma is in a steady state, while TRANSP is fully time dependent. The ρ_* scan plasmas did achieve steady state so both codes have been used, and they produce the same trends — although there are minor differences in the individual simulations. The results shown here are based on the TRANSP analyses, which have more complete modeling of fast ion finite orbit width effects and fast ion charge exchange losses.

The inputs to the analysis codes are the electron density profile measured by a multichannel infrared interferometer, the electron temperature profile determined by a single time multipoint Thomson scattering system, the ion temperature profile based on charge exchange recombination

spectroscopy, and the radiated power profile derived by inverting the signals from multichannel views. We assume a radially constant $Z_{\rm eff}$, its value is derived from the visible bremsstrahlung emitted along a tangential sightline; the metallic contribution to $Z_{\rm eff}$ is determined by soft X-ray spectral analysis.

The analysis codes estimate the fast ion fueling and collisional heating of electrons and thermal ions by simulating neutral beam deposition and thermalization (including orbit losses and fast ion charge exchange). Particle fueling by the limiter gas influx is calculated from a neutral transport simulation which is normalized by the measured brightness of the H_α emission in front of the limiter.

III. HYBRID PREDICTION

The hybrid predictive method for testing transport models combines the strengths of both transport analysis and fully predictive simulation.

Transport analysis infers diffusivities from the measured plasma profiles and a calculation of the heating power profile (this is carried out by codes such as TRANSP, ONETWO [25], SNAP, etc.). Unfortunately, the diffusivities typically have large uncertainties. Using experimentally estimated temperature gradients to evaluate theoretical expressions for diffusivities can create even larger uncertainties and comparison of the two uncertain diffusivities is seldom fruitful.

A fully predictive simulation (by codes such as BALDUR [26], ONETWO [25], and WHIST [27]) uses a transport model in solving diffusion equations to generate predictions of the internal plasma properties such as density, temperature, and internal magnetic field. These predictions can be compared to directly measured quantities, such as temperatures, which have relatively well characterized uncertainties. Unfortunately, the predictions may have a sensitive dependence on details such as the shape of the predicted density or $Z_{\rm eff}$ profiles. Simulation errors which are correlated with ρ_* will influence the apparent ρ_* dependence of the predictions. For example, if the simulated density profile is flatter than the measured profile at low ρ_* and more peaked at high ρ_*, this will tend to compensate for the errors of a transport model with gyroBohm scaling. Thus, imperfections of fully predictive simulations can alter the ρ_* dependence in the same way that experimental imperfections can taint the experimental scalings.

The hybrid prediction method partially mitigates this feature of the predictive approach by relying on measured data as much as possible, but it retains the convenience of comparing the prediction to the directly measured temperatures. The uncertainties in the measured quantities cause corresponding uncertainties in the predicted temperatures, but it is relatively easy to determine the magnitude of these effects by varying these inputs.

The temperatures are predicted by solving the conventional power balance equations,

$$\frac{\partial(1.5nT)}{\partial t} = -\frac{1}{r}\frac{\partial}{\partial r}\left(rq\right) + Q,$$

where

$$Q_e = Q_{\rm b,e} + Q_{\rm ICRH,e} - Q_{\rm rad} + Q_{\rm ie} + Q_{\rm OH},$$

$$Q_i = Q_{\rm b,i} + Q_{\rm ICRH,i} - Q_{\rm cx} - Q_{\rm ie},$$

and the power flows are

$$q_e = -n_{\rm e}\chi_{\rm e}\frac{\partial T_{\rm e}}{\partial r} + 1.5T_{\rm e}\Gamma,$$

$$q_i = -n_{\rm i}\chi_{\rm i}\frac{\partial T_{\rm i}}{\partial r} + 1.5T_{\rm i}\Gamma.$$

In our hybrid methodology the measured density and temperatures are used to calculate the heating and particle source terms (the temperature prediction code reads these from the SNAP

or TRANSP archives). The measured plasma density, $Z_{\rm eff}$, etc., are also used where needed in solving the steady state power balance equations. The measured temperatures are used for the outer boundary conditions. The predicted electron and ion temperatures are used to calculate the theoretical thermal diffusivities, the ion-electron temperature equilibration power, and the convected power. The thermal transport model for a single species can be tested by fixing the temperature of the other species to the measured value.

In the high density TFTR ρ_* scan the convected power is large near the plasma edge. Although it is directly related to the measured H_α emission, the convection is rather uncertain so we specify the outer boundary condition at $r = 0.8a$, and predict the temperatures inside this radius.

IV. RESULTS

We wish to determine whether the ρ_* scaling of the predictions differs from that of the experiments. This is accomplished by examining ρ_* dependence of the goodness of fit of the predictions. A theory which always predicts temperatures which are 20% lower than measured will, nevertheless, possess the correct ρ_* scaling. This means that constant 'scale' errors — in the diagnostics or theories — have little effect on the ρ_* dependence of the measured or predicted transport. Conversely, a theory which predicts temperatures which are 15% low at one end of a scan and 15% high the other end is not acceptable if the uncertainty of the measured temperatures is only 10%. Several transport models predict temperatures 'close' to those measured in a number of tokamaks, but the models tested here fail to pass the more stringent test posed by the ρ_* scans.

The goodness of fit measure shown in the figures is the ratio of predicted to measured temperature at $r = 3a/8$. This is at the location of the first measurement of $T_{\rm i}$ which is outside the region affected by sawteeth. In most cases the difference between prediction and measurement grows steadily as the comparison location moves inward from the outer boundary condition where the prediction is tied to the measured temperature (Fig. 1). The temperature ratio at other radii exhibits very similar trends but the range of variation is reduced as the comparison radius approaches the outer boundary. As a result, the temperature ratio averaged over $3/8 < r/a < 0.7$ is very similar to the figures shown here but the range of variation is slightly less. This also holds true for the the ratio of the predicted and measured thermal stored energies integrated over the entire plasma volume. Thus, comparing the temperatures at a single point is representative of the overall goodness of fit of the predicted profiles.

The measured ratio of ion to electron temperatures was held reasonably constant in all but one plasma: the high ρ_* shot in the low density ρ_* scan. The cause of the unusual ratio of *measured* ion to electron temperatures might be measurement error or variability in some parameter which has an important effect on the transport. We have found no apparently correlated variation in some other parameter which might 'explain' the peculiarity of this shot. It is also peculiar in all the simulations: the ratio of predicted to measured ion temperature does not follow the trend of the other shots in the scan. For completeness it is included in the figures but we ignore it when drawing conclusions about trends.

A. DIII-D Experimental L-mode ρ_* Scalings

We have tested two ρ_* scalings derived from L-mode experiments in the DIII-D tokamak. The first is derived from a number of experiments with high q [12]. The second scaling is obtained from an experiment with lower q [14], in which the ion scaling differed. The inferred $\chi_{\rm i}$ and $\chi_{\rm e}$ for a single shot in each ρ_* scan are scaled to the conditions of the other shots and used to predict their temperatures. The resulting ρ_* trends are independent of the choice of basis shot. We have scaled the diffusivities using either the experimentally measured $T_{\rm e}$ or the predicted $T_{\rm e}$. Using the predicted temperature generates 'negative feedback' by raising the diffusivity, which reduces the difference between the predicted and measured temperature. This is similar to the way transport model diffusivities are tested, so the results for this method are shown here.

The DIII-D high q L-mode ρ_* scaling [12] has gyroBohm scaling of χ_e and Goldston scaling of χ_i. The diffusivities are thus given by

$$\chi_e = (\frac{T_e}{T_e^{ref}})^{1.5}(\frac{B_{tor}^{ref}}{B_{tor}})^2\chi_e^{ref},$$

$$\chi_i = (\frac{T_e}{T_e^{ref}})^{0.75}(\frac{B_{tor}^{ref}}{B_{tor}})^{0.5}\chi_i^{ref},$$

where the reference values are taken from shots 50904 and 56289 in the TFTR ρ_* scans [4]. The predicted temperatures are in good agreement with the measurements (Fig. 2).

The TFTR experiments have edge $q = 3.1$ which is closer to the that in the DIII-D low q experiment, which found that the ion scaling was Bohm-like (while the electrons remained gyroBohm). This ion diffusivity is obtained from

$$\chi_i = (\frac{T_e}{T_e^{ref}})(\frac{B_{tor}^{ref}}{B_{tor}})\chi_i^{ref},$$

where the reference values are again taken from shots 50904 and 56289. The low q scaling is apparently more relevant to the TFTR experiments, but the fit to the TFTR data is not as close (Fig. 3).

In the high density TFTR ρ_* scan the density profile shapes are much flatter than those in the DIII-D discharges, so the relevance of the DIII-D scalings is open to question since these scalings are intended to capture only the ρ_* dependence of the diffusivities. We note, however, that in the low density TFTR ρ_* scan the density profile shapes are similar to those of the DIII-D low q discharges, and the ρ_* trends for *both* TFTR scans are indistinguishable. The degree to which the different experiments *should* be compatible with each other is, ultimately, a question that can only be answered in the context of a full understanding plasma transport; this context can be provided by theory, but it is model dependent.

B. Transport Model Predictions

The Rebut-Lallia-Watkins model [15] (RLW) features a critical electron temperature gradient that enters into the heat flux of both electrons and ions. As previously shown [16], temperature predictions for this model are in clear disagreement with the TFTR experiments (Fig. 4). The ρ_* scaling is gyroBohm in both the electron and ion channels, and the temperature gradients in the TFTR discharges are well above the critical gradient [4] so the predictions should exhibit full gyroBohm scaling. The strong ρ_* trends are, indeed, quite similar to those obtained using 'naive' gyroBohm scaling for both the electrons and the ions (using the simulation method described in the previous section).

In response to the ρ_* scaling experiments in TFTR [4] and DIII-D [11], Boucher [16] modified the RLW model to give the ion diffusivity Bohm scaling. He found that this improved the fit to the data but a significant ρ_* trend remains [16] (Fig. 5). The ρ_* scaling of this model is identical to the DIII-D low q L-mode scaling: gyroBohm electrons and Bohm ions. The markedly stronger ρ_* trend in the ion temperatures predicted by the RLWB model may be due its suppression of both diffusivities as T_i rises.

The Institute for Fusion Studies-Princeton Plasma Physics Laboratory (IFS-PPPL) model is derived from numerical simulations of toroidal ion temperature gradient (ITG) turbulence [28]. It has no parameters which are determined by comparing predictions to data; it is thus a purely theory based model. It also has gyroBohm scaling of both χ_e and χ_i, but the critical temperature gradient is in the ion temperature. Its predictions (Fig. 6) have a less marked ρ_* trend than the RLW or the 'naive' double gyroBohm model. Note that its predictions are more reliable at the low ρ_* end of the scans, which are in the typical L-mode operating regime of TFTR where the predictions of the IFS-PPPL ITG model are in accord with many TFTR L-mode plasmas [28].

The predictions fall well below the measurements in three higher ρ_* discharges, all of which have unbalanced neutral beam injection. The resulting plasma rotation is sufficient to greatly reduce the diffusivities, according to preliminary estimates of sheared flow stabilization [29]. The extent to which plasma rotation affects the diffusivities has a very strong correlation with ρ_* since unidirectional injection was used in the lowest power shots with a single ion source.

A more detailed study of the influence of sheared flows is being carried out. The effects of both stabilizing $E \times B$ shear and destabilizing parallel flow shear will be included in nonlinear gyrofluid simulations.

C. Sources of Uncertainty

We now turn to a discussion of whether the predictions depart significantly from the apparent ρ_* dependence of the experiments. In other words, is the ratio of predicted to measured temperature constant to within the uncertainty of this quantity? The sources of uncertainty are discussed below in three categories: 1) uncertainties in the measured temperatures, 2) the effect of measurement uncertainties on the predicted temperatures, and 3) uncertainties arising from the modeling algorithms.

The ion temperature in TFTR is measured by a multichannel charge exchange recombination spectroscopy system [30]. The relative uncertainty depends chiefly on the number of beamlines contributing to the signal; the discharges with low heating power therefore have a lower signal to noise ratio. The 1σ uncertainty at the comparison radius varies from $\sim$10% at high ρ_* to $\sim$5% at low ρ_* for both of the scans. The uncertainty rises to 15–35% where the boundary condition is imposed on the predictions.

The electron temperatures were measured by a Thomson scattering system [31]; in these plasmas the uncertainties are dominated by photon statistics. At both the comparison radius and the location of the outer boundary condition, the 1σ uncertainties are $\sim$10% for all but the two highest density discharges, where they are 4–5%.

The measured temperature is used to set the boundary condition when solving the power balance equations to obtain the predicted temperatures. Changing the ion temperature boundary condition produces a T_i offset (relative to the nominal prediction) which propagates into the solution region. The 1σ uncertainty in T_i is 70–100 eV at the boundary. For the DIII-D scalings as well as the RLW and RLWB models, the offset at the comparison radius has shrunk to 30–50 eV; the uncertainty in the predicted T_i there is 2–5%. The uncertainty in the T_i boundary value causes an uncertainty in the predicted T_e at the comparison radius of only $\sim$2%. For the IFS-PPPL predictions, the ion temperature offset increases toward the interior of the plasma in the low density scan, but it is nearly constant in the high density scan. The 1σ uncertainty in the boundary ion temperature changes the predicted ion temperature at $r = 0.3$m by 17% at high ρ_* and 5% at low ρ_*. The larger T_i offset found with this model creates larger uncertainty in predicted T_e, it varies from 15% to 4% at the comparison radius.

The strong T_e dependence of χ_e in all theoretical models and the DIII-D scalings leads to negative feedback which quickly diminishes T_e offsets created by changing the electron temperature boundary value. The predicted electron temperature is quite 'resilient': the measurement uncertainties in T_e at the boundary make predictions of T_e at the comparison radius uncertain by <2% for the theoretical models, and up to 6% for the DIII-D scalings. The effect on the predicted T_i is also typically <3% .

The uncertainty in the neutral beam absolute power calibration is 15%, but the source to source variation in power is only $\sim$5% (the precision is limited by the measurement uncertainties in the calorimetry). A single neutral beam source was used for one discharge, and at the high power end of the scans 8 or 9 sources were injected. The relative uncertainty in the injected power across the ρ_* scan is thus $\sim$5%. Changing the heating power by 5% changes the predicted temperatures by only 2–3%, typically. This insensitivity is caused by the temperature dependence of the diffusivities, which partially offsets the change in heating power. The ion temperatures predicted by the IFS-PPPL transport model were remarkably insensitive to variations in the heating power: the changes were only 1%.

The density gradient plays a direct role in the theoretical transport models, so the effect of uncertainties in the measured density profile are of interest. Over distances which are small compared to the minor radius, a, the uncertainty in the density gradient is quite large, but errors must extend over a large fraction of a in order to produce a significant change in the temperature. For this sensitivity study we have scaled the density by the factor

$$F(r) = 1 + \epsilon - 2\epsilon r/a,$$

which changes the density scale length by

$$\Delta L_{\rm n}^{-1} \sim \pm 2\epsilon/a.$$

It is difficult to quantify the large scale errors in the measured density profile because they arise from errors in modeling the poorly diagnosed scrape off layer. Nevertheless, we feel that $\epsilon = \pm 0.1$ corresponds to a generous upper bound on this uncertainty. Using the density modifications described above, we find that the predicted temperatures vary by only 2–5% for the RLW and RLWB models, and only 2% or less for the IFS-PPPL model. The density gradient has no direct influence on the DIII-D scalings so their predicted temperatures changed by less than 1%.

Finally, we note the effect on the predictions of Monte Carlo noise in the TRANSP simulation of neutral beam heating, the effects of sawteeth, and the location of the outer boundary condition. Predictions based on heating profiles from five different times in the steady state phase of the TRANSP analysis runs show a scatter of $\sim$2% for both the ion and electron temperatures. The diffusivities inferred by TRANSP are used with the DIII-D scalings; variations in the diffusivities also produce a scatter of $\sim$2% in the predicted temperatures. Our simulations usually ignore the effects of sawteeth, but sawteeth might indirectly affect the temperatures at the comparison radius through their effect on the ion-electron temperature equilibration power. When a large *ad hoc* diffusivity inside the sawtooth mixing radius is used to flatten the temperature profiles there, the temperatures at the comparison radius change by $<$1% for all cases except the IFS-PPPL model $T_{\rm e}$ which rises by $\leq$4% (with no ρ_* trend).

Convection and radiation are important in the power balance near the edge so we locate the outer boundary condition at $r = 0.8a$ to avoid large uncertainties in both terms affecting the predictions. Moving the location of the boundary has effects similar to those of boundary value changes: the difference between ion temperature of the standard prediction and the boundary value at the new location persists as described above for the various transport models, but changes in the electron temperature quickly decay. As a result, the predicted ion temperature tends toward the measured ion temperature as the outer boundary moves toward the comparison radius, but the predicted electron temperature is affected very little until the outer boundary is within $\sim 0.2a$ of the comparison radius.

The total 1σ uncertainty shown in the figures of the ratio of predicted and measured temperatures (Figs. 2-6) is obtained from the experimental measurement uncertainties in the temperatures (at the comparison radius and at the boundary condition location), the beam heating power, the density gradient, and the Monte Carlo noise in the TRANSP analyses.

V. CONCLUSIONS AND DISCUSSION

Of all the models considered here, the scaling obtained from the DIII-D high q L-mode experiments fits the TFTR data best. The small ρ_* trends in the ratio of predicted to measured temperatures are within the measurement uncertainties of both the electron and ion temperatures (Fig. 2). (The discrepant shot 50921 is ignored for the reasons discussed above.)

The DIII-D low q L-mode scaling (with Bohm-like ions) produces somewhat larger ρ_* trends for both electrons and ions (Fig. 3). When the prediction uncertainties are included, the ion temperature ratio remains within the uncertainties. The larger variation in the electron temperature ratio is due to the $Q_{\rm ie}$ power flow from the ions rather than a defect in the scaling for electrons (which is the same as for the high q scaling). When the electron scaling alone is tested (using measured $T_{\rm i}$ in the prediction of $T_{\rm e}$) there is no significant ρ_* trend in the electron temperature ratio.

We find that both the RLW model and Boucher's variant of it (with Bohm-like ion diffusivity) are not compatible with the experimental data. The combined experimental and prediction uncertainties are 15–20% for the highest ρ_* plasmas and ~10% for the lowest ρ_* plasmas. The 90% and 50% variations in the T_i ratio cannot be accommodated (Figs. 4,5). The RLW predictions are quite similar to those for a model in which both electrons and ions have 'naive' gyroBohm scaling (in the same spirit as the DIII-D scalings). Once again, the ρ_* trends for the electron temperature ratio are caused by Q_{ie} coupling to the incorrectly predicted ion temperatures. When the electron scaling alone is tested (using measured T_i in the prediction of T_e) there is no significant ρ_* trend in the electron temperature ratio.

It is interesting to note that the low q DIII-D scaling and the RLWB transport model share the same ρ_* dependences: each has gyroBohm electrons and Bohm-like ions The rather different ρ_* trends of the predictions show that the formal ρ_* dependence is not the whole story. The different trends are presumably caused by the effect of the experimental imperfections on the more complex RLWB model. The variations in the density profile shape, in particular, contribute to the observed ρ_* trend.

The ρ_* variation of the ion temperature ratio for the IFS-PPPL model (Fig. 6) is nearly 50%. The combined experimental and prediction uncertainties are 20% for the highest ρ_* plasmas and ~10% for the lowest ρ_* plasmas. Although this model has the largest sensitivity to errors in the boundary value of the ion temperature, the variation is outside the range of uncertainty. The ratio of electron temperatures exhibits no clear ρ_* trend.

The IFS-PPPL model is being extended to include the effects of sheared flows. Preliminary estimates show that it will very substantially alter the predictions for the discharges which are not well modeled by the original formulation of the model (those with unbalanced neutral beam injection). At present, the uncertainty in the effects of sheared flows is relatively large so we do not consider the matter further here.

VI. SUMMARY

The ρ_* scalings obtained from nondimensional L-mode experiments in DIII-D are consistent with the measured temperatures in the TFTR ρ_* scans. The high q scaling produces the best fit, but q in the TFTR experiments is closer to that in the low q DIII-D experiments. The low q scaling may fit less well because of the imperfect density profile matching, but this explanation seems unlikely because the two ρ_* scans have differing variations while the ion temperature ratios show the same trends.

All of the theoretically based transport models — Rebut-Lallia-Watkins [15], Boucher's modification of RLW [16], and IFS-PPPL [17] — predict ion temperatures which have incorrect apparent ρ_* dependence. The temperature predictions use the *measured* density profiles (and other quantities) so some of the experimental imperfections of the nondimensional scans are accounted for. As Waltz [18] found previously, the inclusion of these imperfections can alter the apparent ρ_* scaling. This is borne out in the present work by the observation that Boucher's variant of the RLW model does not mimic the DIII-D low q L-mode scaling (which has the same ρ_* dependences), and the fully gyroBohm IFS-PPPL model does not mimic the corresponding 'naive' scaling which depends only on ρ_*. On the other hand, the electron temperature gradient in the TFTR plasmas is well above the RLW critical gradient, and we found that the RLW predictions are close to the naive gyroBohm trends.

The IFS-PPPL predictions differ significantly from the measurements only in three discharges, all of which have unbalanced neutral beam injection. The resulting plasma rotation is sufficient to greatly reduce the diffusivities, according to preliminary estimates of sheared flow stabilization [29]. We also find that sheared flows are important in DIII-D and JET ρ_* experiments. It is an important question whether these effects are important in the context of other theories, as well, but the answer depends on the details of each theory. Inclusion of the effects of sheared flows in the IFS-PPPL transport model is not complete, so a detailed study of the influence of sheared flow stabilization in the TFTR and DIII-D ρ_* scans, and rotation scans in TFTR is deferred to another paper.

VII. ACKNOWLEDGEMENTS

It is a pleasure to thank R. E. Bell, B. Grek, L. R. Grisham, G. W. Hammett, S. M. Kaye, T. C. Luce, A. T. Ramsey, and E. J. Synakowski for enlightening discussions. This work was supported by U.S. Department of Energy Contract No. DE-AC02-76CH03073.

---

[1] R. E. Waltz, J. C. DeBoo, and M. N. Rosenbluth, Phys. Rev. Lett. **65**, 2390 (1990).

[2] P.-H. Rebut, V. Chuyanov, M. Huget, R. R. Parker, and Y. Shimomura, The ITER EDA outline design, in *Plasma Physics and Controlled Nuclear Fusion Research (Proc. Fifteenth Intl. Conf., Seville, 1994)*, volume 2, pp. 451–467, Vienna, 1994, International Atomic Energy Agency.

[3] D. J. Grove and D. M. Meade, Nucl. Fusion **25**, 1167 (1985).

[4] F. W. Perkins, C. W. Barnes, D. W. Johnson, S. D. Scott, M. C. Zarnstorff, M. G. Bell, R. E. Bell, C. E. Bush, B. Grek, K. W. Hill, D. K. Mansfield, H. Park, A. T. Ramsey, J. Schivell, B. C. Stratton, , and E. Synakowski, Phys. Fluids B **5**, 477 (1993).

[5] B. B. Kadomtsev, Sov. J. Plasma Phys. **1**, 295 (1975).

[6] J. W. Connor and J. B. Taylor, Nucl. Fusion **17**, 1047 (1977).

[7] J. W. Connor, Plasma Phys. Controlled Fusion **30**, 619 (1988).

[8] J. W. Connor and H. R. Wilson, Plasma Phys. Controlled Fusion **36**, 719 (1994).

[9] P.-H. Rebut, R. J. Bickerton, and B. E. Keen, Nucl. Fusion **25**, 1011 (1985).

[10] J. L. Luxon and L. G. Davis, Fusion Tech. **8**, 441 (1985).

[11] C. C. Petty, T. C. Luce, and R. I. Pinsker, Low density ech in diii-d, in *Radio-Frequency Power in Plasmas: Tenth Topical Conference (Boston 1993)*, p. 165, Washington, 1994, American Institue of Physics.

[12] C. C. Petty, T. C. Luce, K. H. Burrell, S. C. Chiu, J. S. deGrassie, C. B. Forest, P. Gohil, C. M. Greenfield, R. J. Groebner, R. W. Harvey, R. I. Pinsker, R. Prater, and R. E. Waltz, Phys. Plasmas **2**, 2342 (1995).

[13] J. P. Christiansen, P. M. Stubberfield, J. G. Cordey, C. Gormezano, C. W. Gowers, J. O'Rourke, D. Stork, A. Taroni, and C. D. Challis, Nucl. Fusion **33**, 863 (1993).

[14] T. C. Luce and C. C. Petty, Experimental determination of the dimensionless parameter scaling of energy transport in tokamaks, in *Conference on Controlled Fusion and Plasma Physics (Proc. 22th Int. Conf., Innsbruck, 1992)*, volume 19C, part III, pp. 25–28, Brussels, 1995, European Physical Society, also report GA-A22096.

[15] P.-H. Rebut, M. L. Watkins, D. J. Gambier, and D. Boucher, Phys. Fluids B **3**, 2209 (1991).

[16] M. N. Rosenbluth, J. Hogan, D. Boucher, A. Bondeson, P. Barabaschi, B. Coppi, L. Degtyarev, S. W. Haney, H. Goedbloed, T. C. Hender, H. Holties, G. Huysmanns, W. Kerner, J. Manickam, A. Martynov, S. Medvedev, D. Monticello, T. Ozeki, L. D. Pearlstein, F. Perkins, A. Pletzer, F. Porcelli, P.-H. Rebut, S. Tokuda, A. D. Turnbull, L. Villard, and J. Wesley, ITER plasma modeling and mhd stability limits, in *Plasma Physics and Controlled Nuclear Fusion Research (Proc. Fifteenth Intl. Conf., Seville, 1994)*, volume 2, pp. 517–524, Vienna, 1994, International Atomic Energy Agency.

[17] W. Dorland, M. Kotschenruther, M. A. Beer, G. W. Hammett, R. E. Waltz, R. R. Dominguez, P. M. Valanju, W. H. Miner, Jr., J. Q. Dong, W. Horton, F. L. Waelbroeck, T. Tajima, and M. J. LeBrun, Comparisons of nonlinear toroidal turbulence simulations with experiment, in *Plasma Physics and Controlled Nuclear Fusion Research (Proc. Fifteenth Intl. Conf., Seville, 1994)*, volume 3, pp. 463–474, Vienna, 1994, International Atomic Energy Agency.

[18] R. E. Waltz, J. E. DeBoo, and T. H. Osborne, Nucl. Fusion **32**, 1051 (1992).

[19] J. E. Kinsey and G. Bateman, Phys. Plasmas **3**, 3344 (1996).

[20] H. Nordman, P. Strand, J. Weiland, A. Jarmen, and J. P. Christiansen, Drift wave transport simulations of JET gyro-radius scaling experiments, in *Plasma Physics and Controlled Nuclear Fusion Research (Proc. Sixteenth Intl. Conf., Montreal, 1996)*, Vienna, 1996, International Atomic Energy Agency, paper IAEA-CN-64/DP-8.

[21] R. J. Hawryluk, in *Physics of Plasmas Close to Thermonuclear Conditions (Proc. Course Varenna, 1979)*, volume 1, p. 19, Commision of the European Communities, Brussels, 1980.

[22] R. J. Goldston, in *Basic Physical Processes of Toroidal Fusion Plasmas (Proc. Course and Workshop Varenna, 1985)*, volume 1, p. 165, Monotypia Franchi, Perugia, 1986.
[23] M. C. Zarnstorff, K. McGuire, M. G. Bell, B. Grek, D. Johnson, D. McCune, H. Park, A. Ramsey, and G. Taylor, Phys. Fluids B **2**, 1852 (1990).
[24] H. H. Towner, R. J. Goldston, G. W. Hammett, J. A. Murphy, C. Kieras-Phillips, S. D. Scott, M. C. Zarnstorff, and D. Smithe, Rev. Sci. Instrum. **63**, 4753 (1992).
[25] H. St. John, T. S. Taylor, Y. R. Lin-Liu, and A. D. Turnbull, Transport simulation of negative magnetic shear discharges, in *Plasma Physics and Controlled Nuclear Fusion Research (Proc. Fifteenth Intl. Conf., Seville, 1994)*, volume 3, pp. 603–614, Vienna, 1994, International Atomic Energy Agency.
[26] C. E. Singer, D. E. Post, D. R. Mikkelsen, M. Redi, A. McKenney, A. Silverman, F. G. P. Seidl, P. H. Rutherford, R. J. Hawryluk, W. D. Langer, L. Foote, D. B. Heifetz, W. Houlberg, M. Hughes, R. Jensen, G. Lister, and J. Ogden, Computer Phys. Comm. **49**, 275 (1988).
[27] W. Houlberg, S. Attenberger, and L. Hively, Nucl. Fusion **22**, 935 (1982).
[28] M. Kotschenreuther, W. Dorland, M. A. Beer, and G. W. Hammett, Phys. Plasmas **2**, 2381 (1995).
[29] G. W. Hammett, 1995, private communication.
[30] R. E. Bell, D. W. Johnson, B. C. Stratton, and E. J. Synakowski, Rev. Sci. Instrum. **63**, 4744 (1992).
[31] B. Grek, 1996, private communication.

Figure captions

1) The measured (solid) and predicted temperature profiles for TFTR shot 52504. Predictions are based on the RLW model (short dashes), the RLWB model (dash-dot), and the IFS-PPPL model (long dashes).

2) Ratio of predicted to measured temperatures for the DIII-D high q L-mode scaling: a) T_e, b) T_i. The circles are the TFTR low density ρ_* scan, the triangles are the high density scan.

3) Ratio of predicted to measured temperatures for the DIII-D low q L-mode scaling: a) T_e, b) T_i. The circles are the TFTR low density ρ_* scan, the triangles are the high density scan.

4) Ratio of predicted to measured temperatures for the Rebut-Lallia-Watkins model: a) T_e, b) T_i. The circles are the TFTR low density ρ_* scan, the triangles are the high density scan.

5) Ratio of predicted to measured temperatures for the Rebut-Lallia-Watkins-Boucher model: a) T_e, b) T_i. The circles are the TFTR low density ρ_* scan, the triangles are the high density scan.

6) Ratio of predicted to measured temperatures for the IFS-PPPL model: a) T_e, b) T_i. The circles are the TFTR low density ρ_* scan, the triangles are the high density scan. Preliminary estimates of the effects of sheared flow stabilization (not shown) bring the low points into agreement with the measurements.

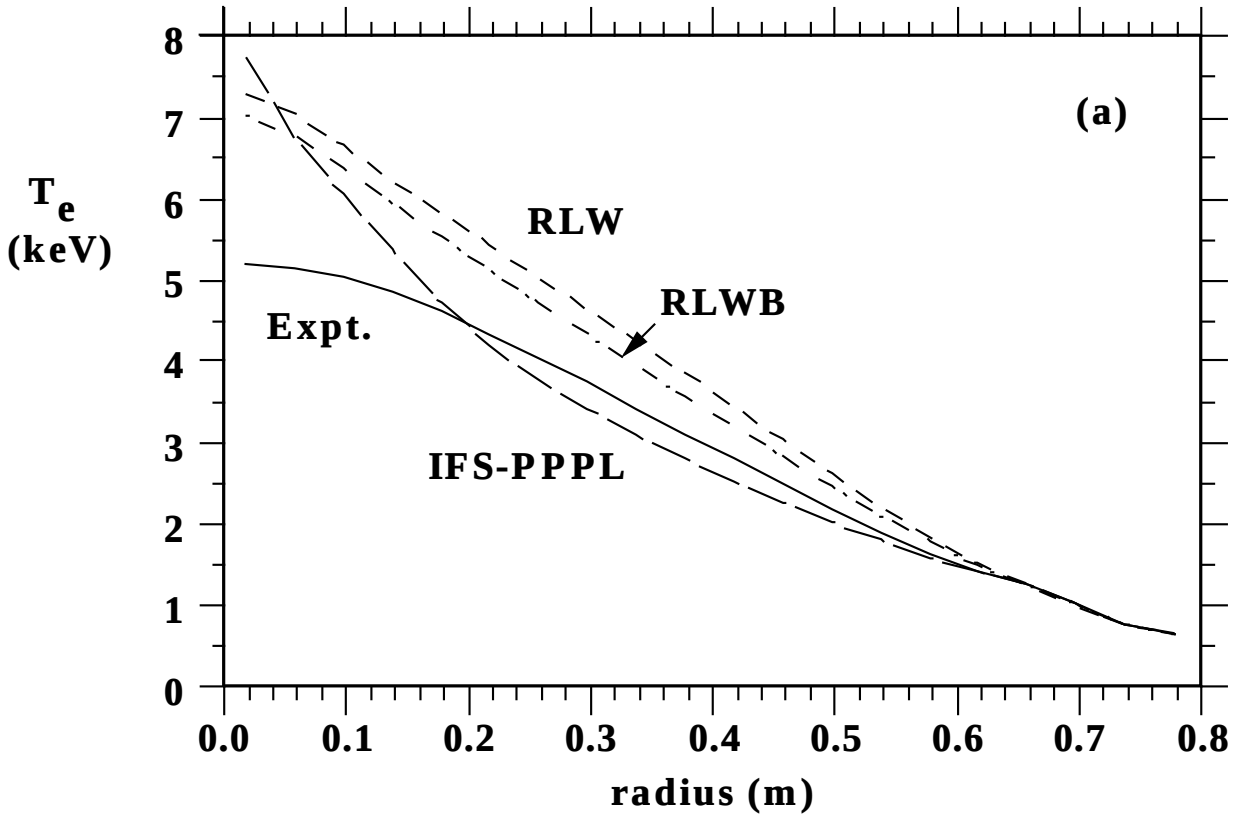
(a)
T_e (keV)
RLW
RLWB
Expt.
IFS-PPPL
0
1
2
3
4
5
6
7
8
0.0
0.1
0.2
0.3
0.4
0.5
0.6
0.7
0.8
radius (m)

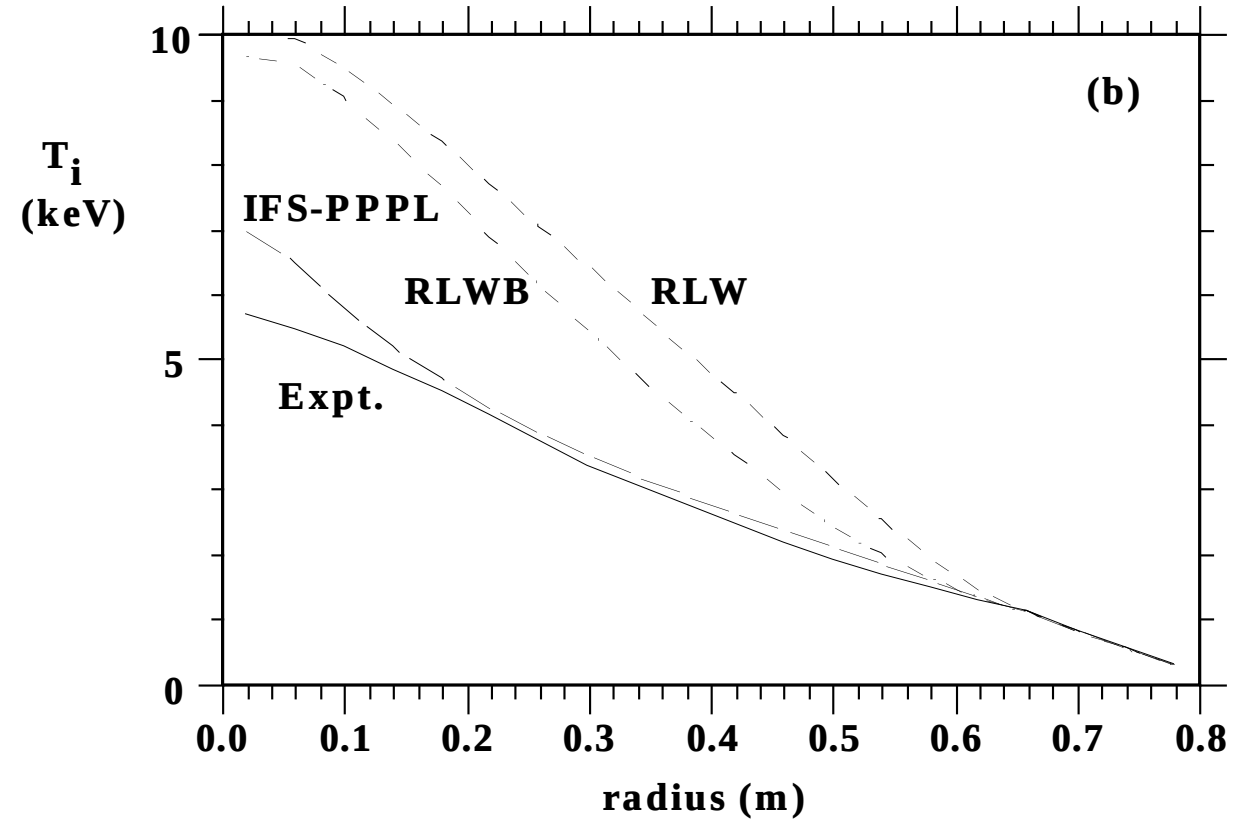
(b)
T_i (keV)
IFS-PPPL
RLWB
RLW
Expt.
0
5
10
0.0
0.1
0.2
0.3
0.4
0.5
0.6
0.7
0.8
radius (m)

Fig. 1

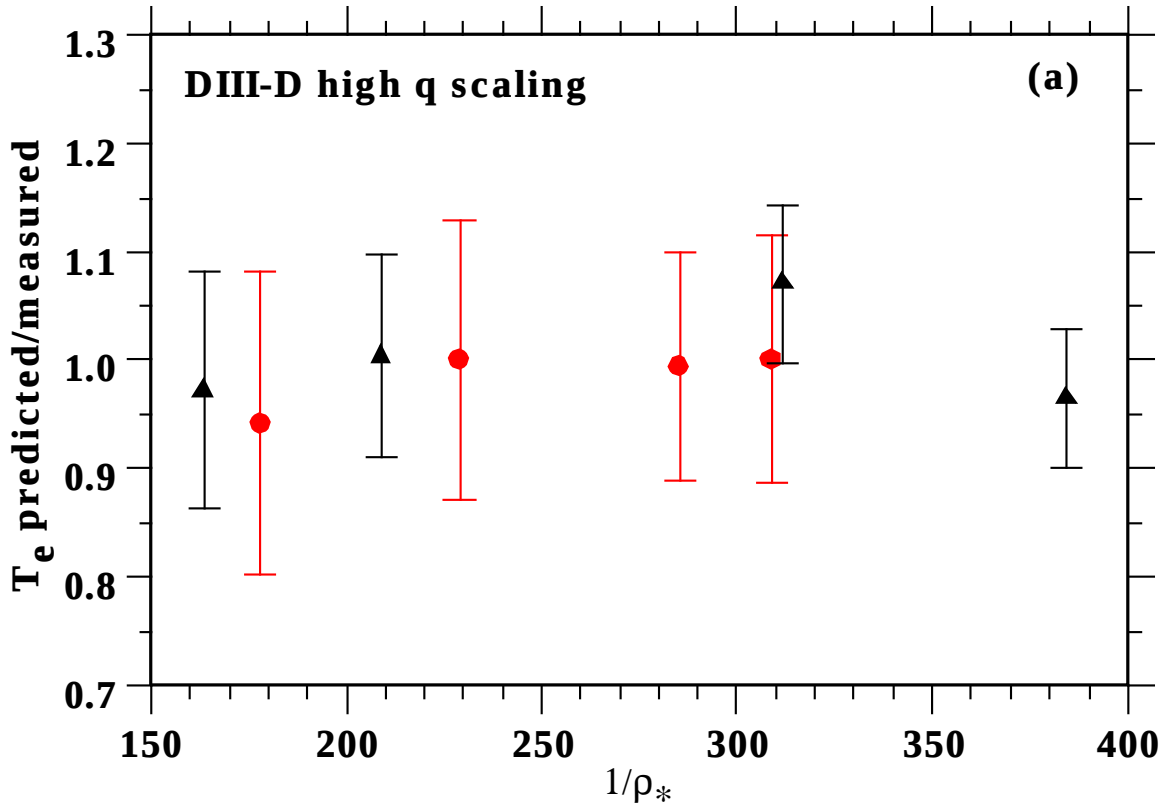
DIII-D high q scaling
(a)
T_e predicted/measured
1.3
1.2
1.1
1.0
0.9
0.8
0.7
150
200
250
300
350
400
$1/\rho_*$

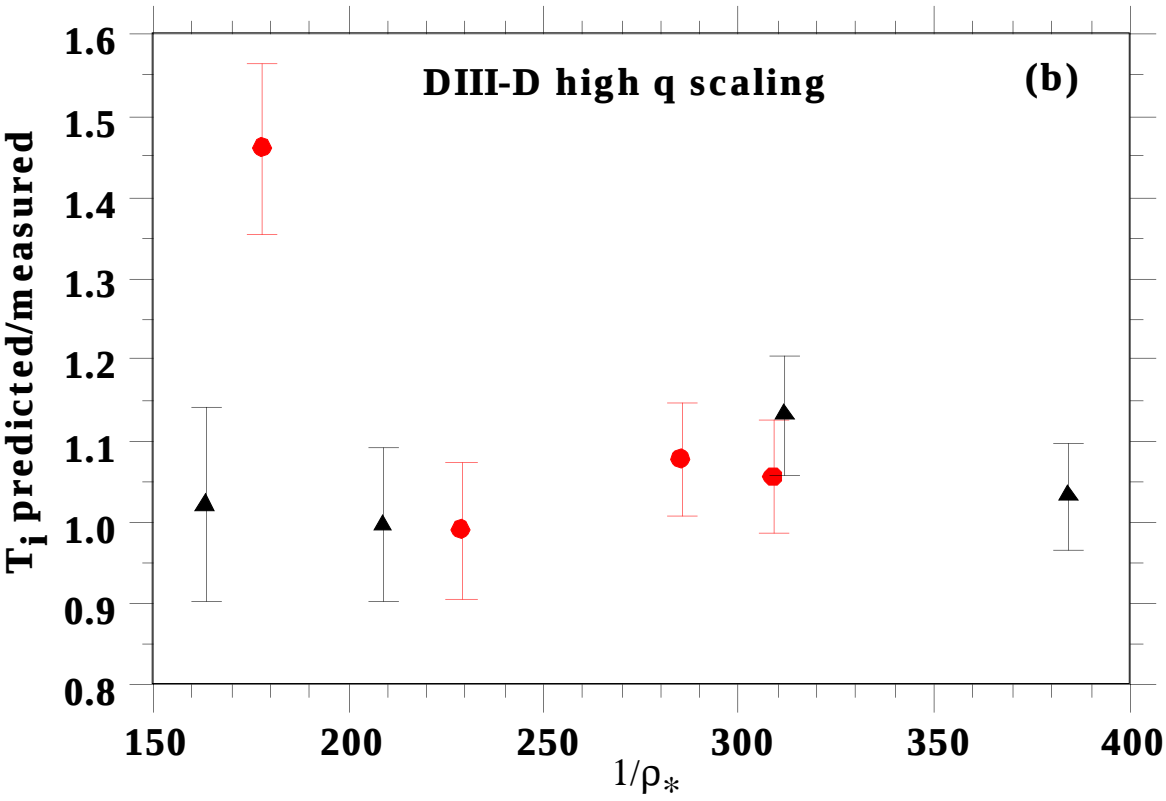
DIII-D high q scaling
(b)
T_i predicted/measured
1.6
1.5
1.4
1.3
1.2
1.1
1.0
0.9
0.8
150
200
250
300
350
400
$1/\rho_*$

Fig. 2

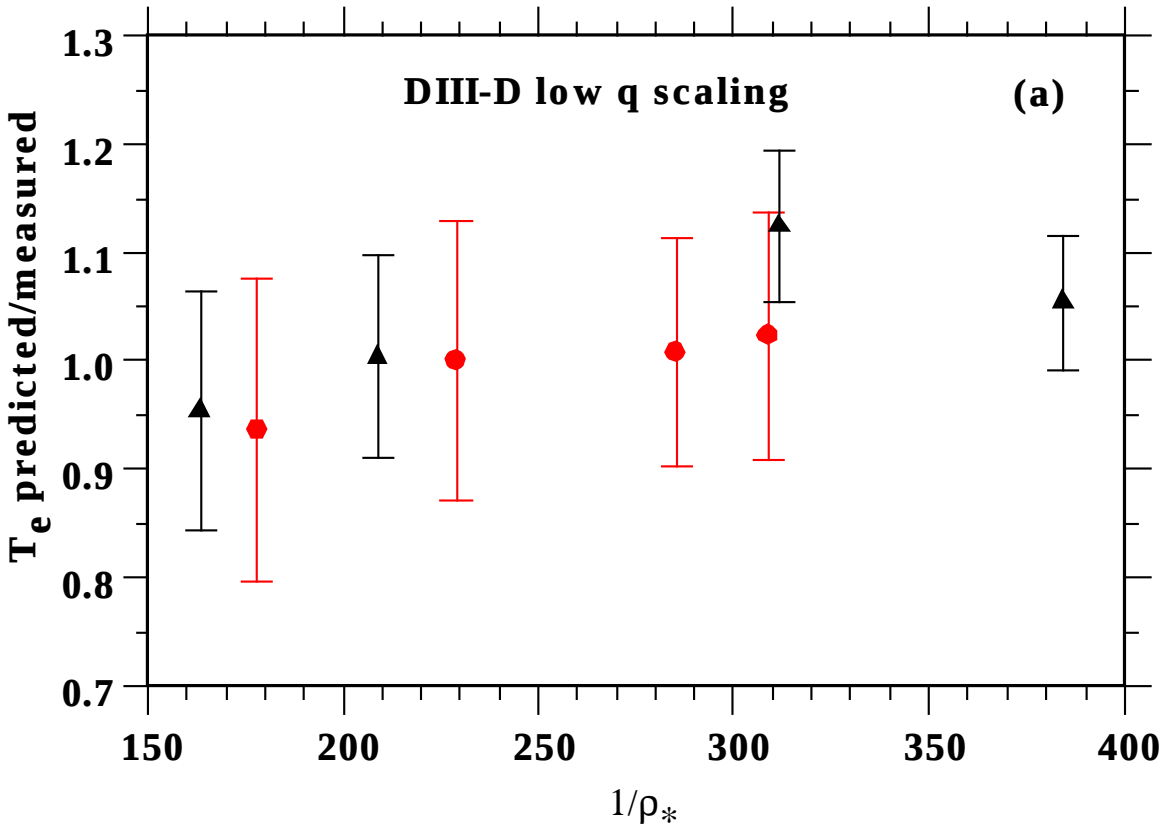
DIII-D low q scaling
(a)
T_e predicted/measured
1.3
1.2
1.1
1.0
0.9
0.8
0.7
150
200
250
300
350
400
$1/\rho_*$

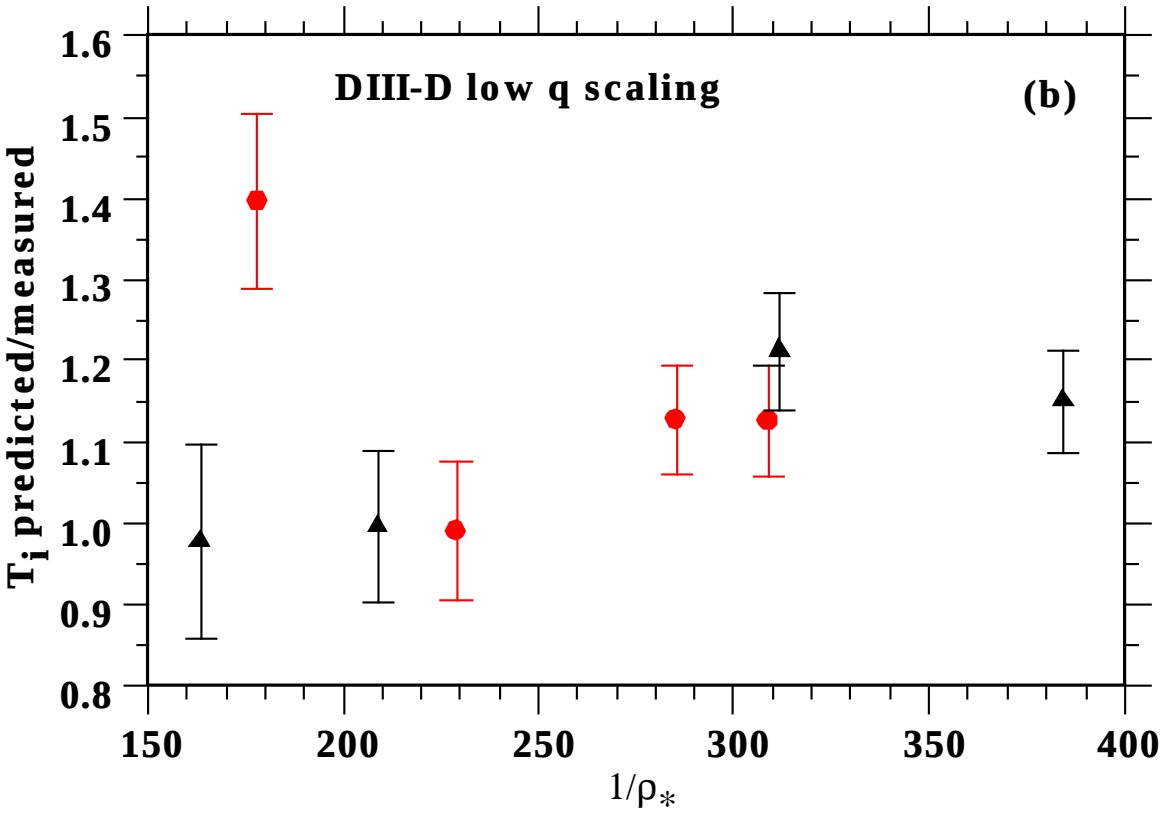
DIII-D low q scaling
(b)
T_i predicted/measured
1.6
1.5
1.4
1.3
1.2
1.1
1.0
0.9
0.8
150
200
250
300
350
400
$1/\rho_*$

Fig. 3

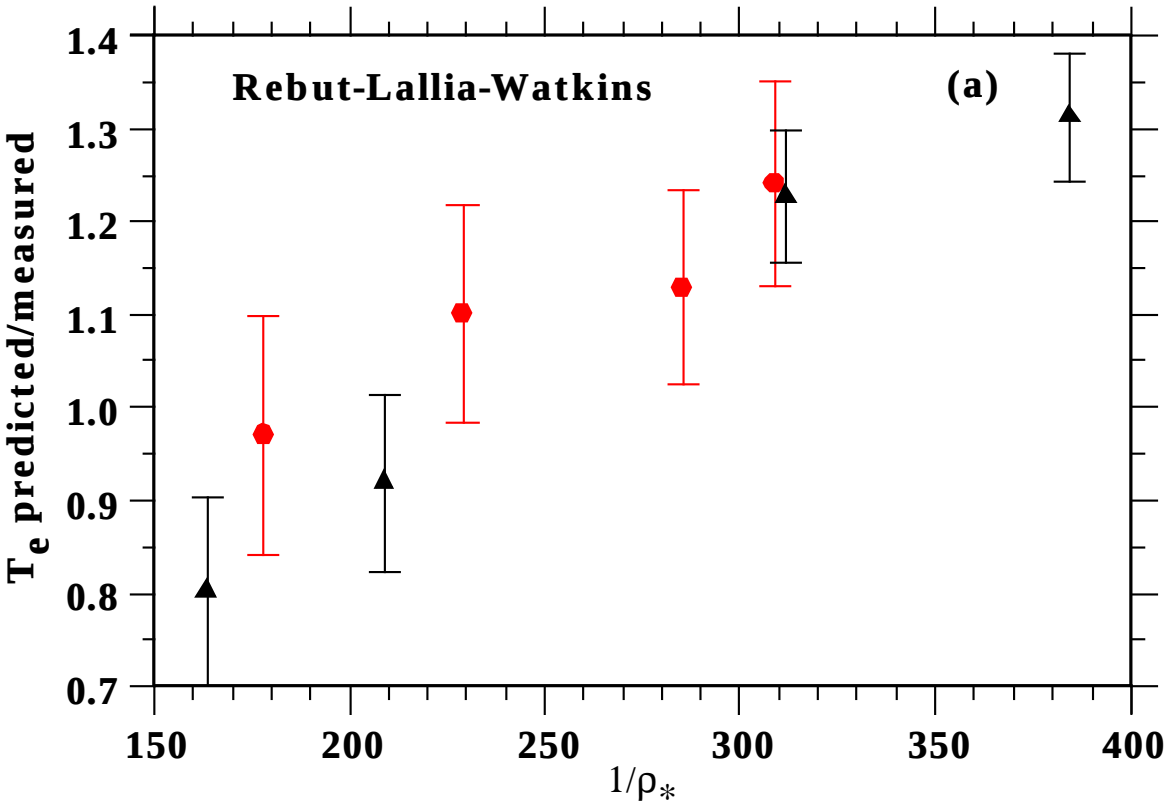
Rebut-Lallia-Watkins
(a)
T_e predicted/measured
1.4
1.3
1.2
1.1
1.0
0.9
0.8
0.7
150
200
250
300
350
400
$1/\rho_*$

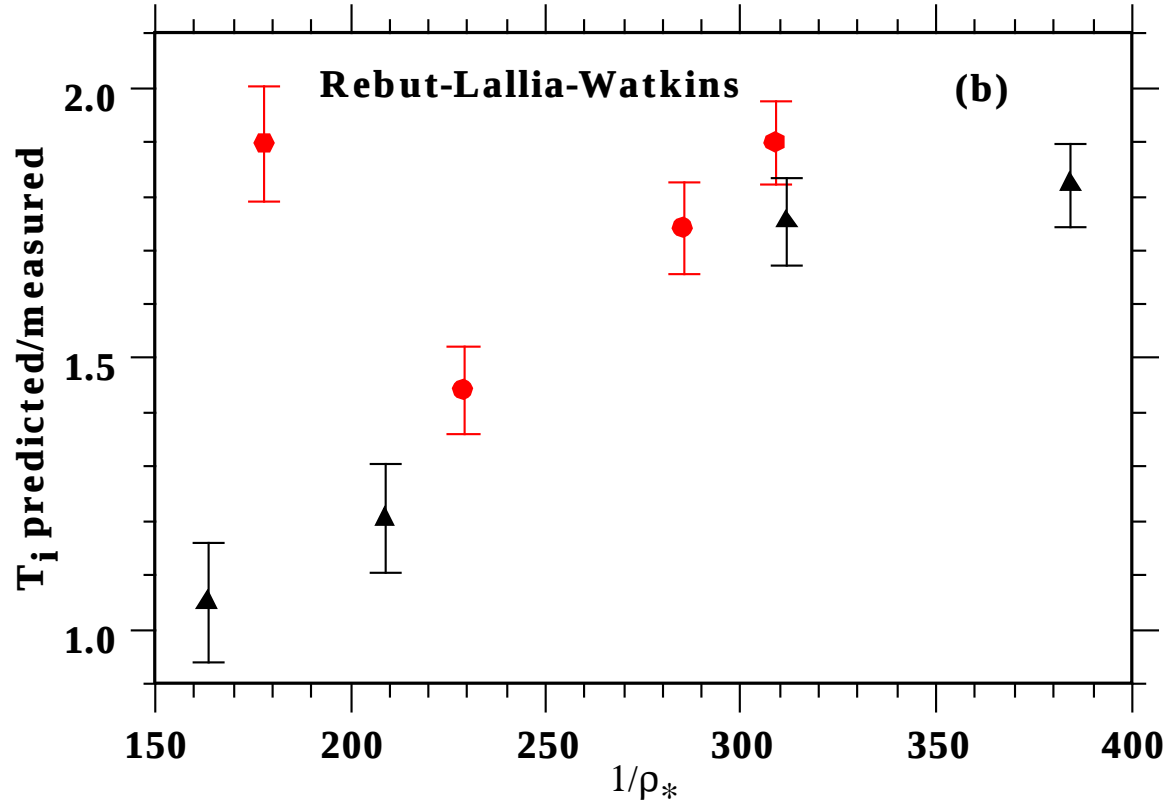
Rebut-Lallia-Watkins
(b)
T_i predicted/measured
2.0
1.5
1.0
150
200
250
300
350
400
$1/\rho_*$

Fig. 4

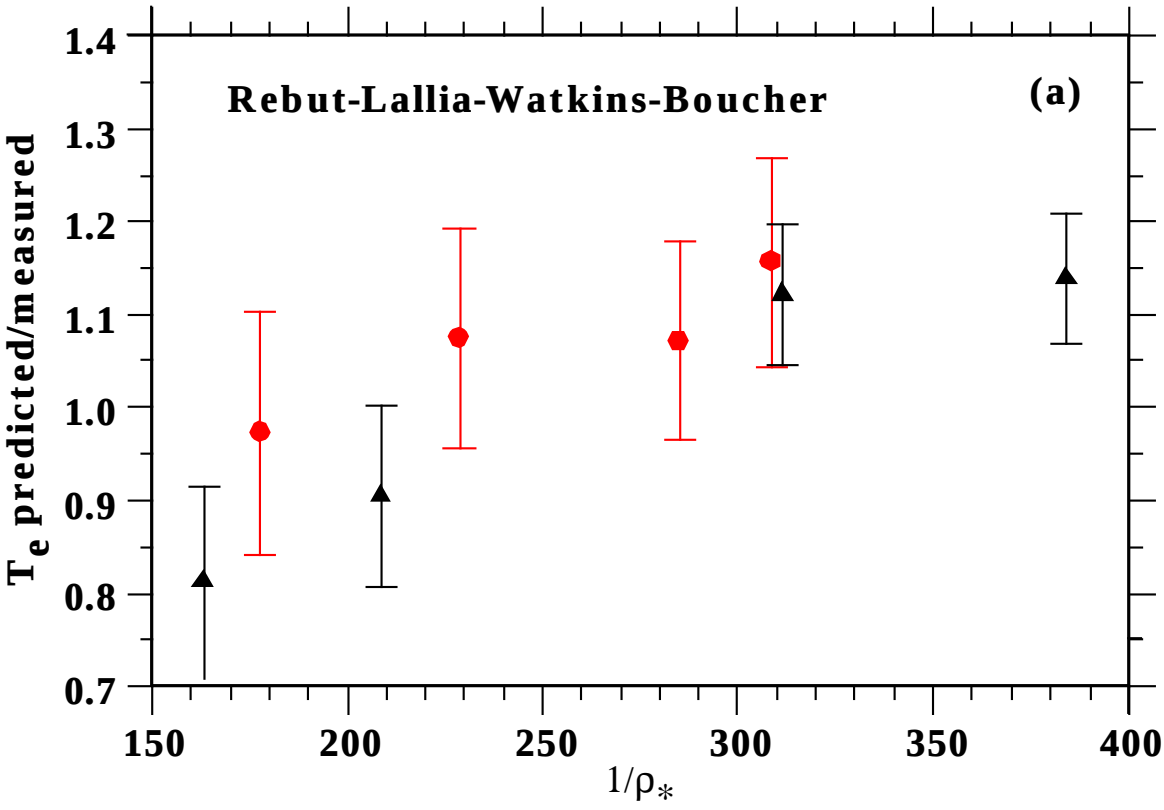
Rebut-Lallia-Watkins-Boucher
(a)
T_e predicted/measured
1.4
1.3
1.2
1.1
1.0
0.9
0.8
0.7
150
200
250
300
350
400
$1/\rho_*$

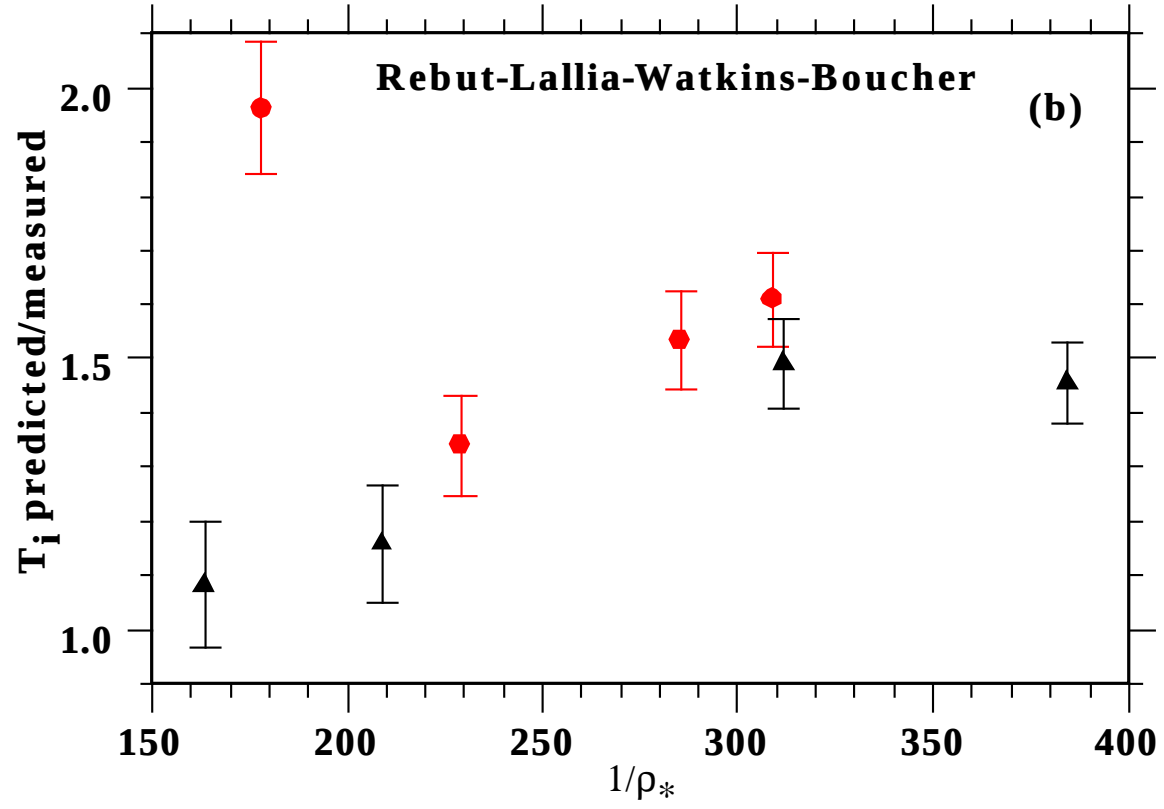
Rebut-Lallia-Watkins-Boucher
(b)
T_i predicted/measured
2.0
1.5
1.0
150
200
250
300
350
400
$1/\rho_*$

Fig. 5

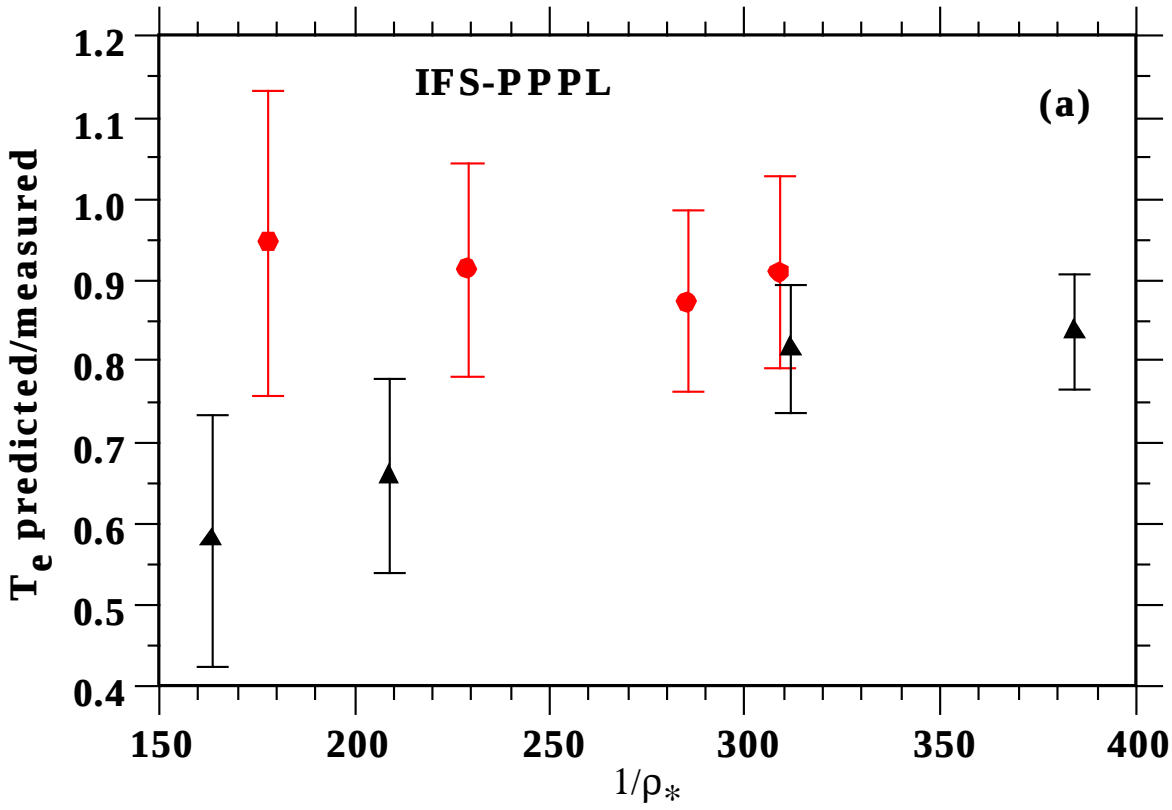
IFS-PPPL
(a)
T_e predicted/measured
1.2
1.1
1.0
0.9
0.8
0.7
0.6
0.5
0.4
150
200
250
300
350
400
$1/\rho_*$

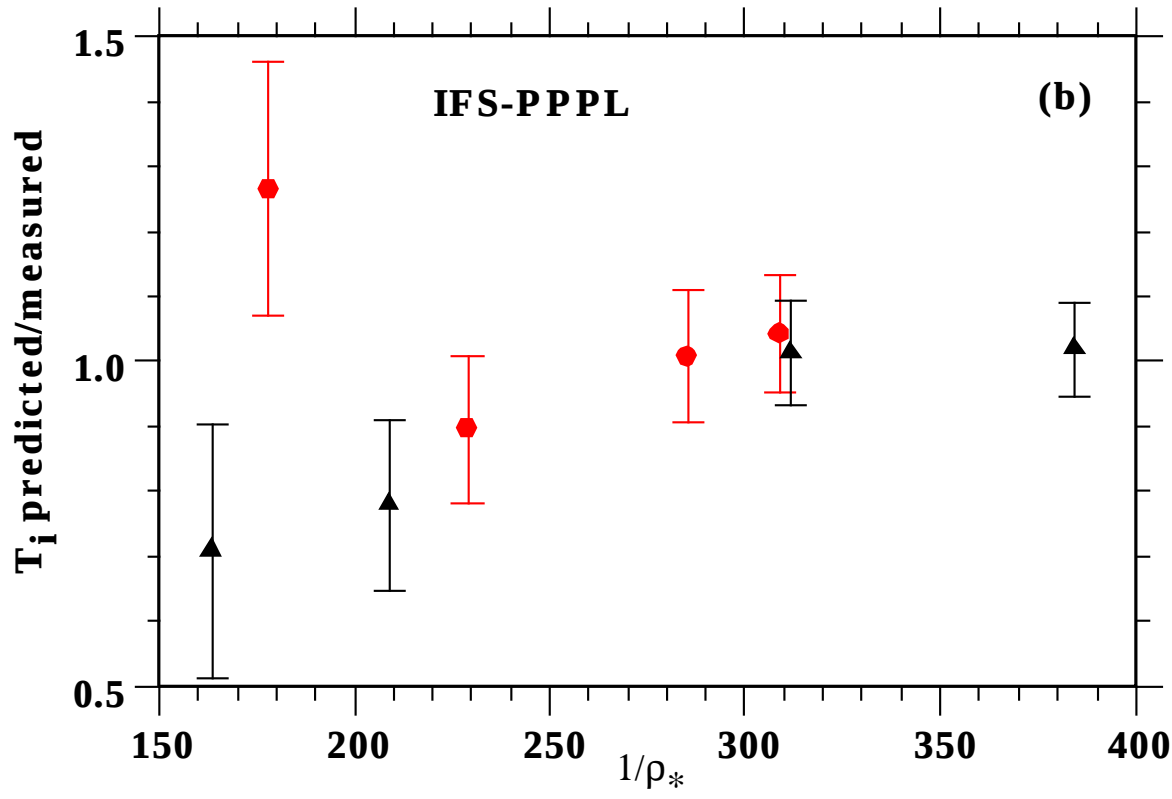
IFS-PPPL
(b)
T_i predicted/measured
1.5
1.0
0.5
150
200
250
300
350
400
$1/\rho_*$

Fig. 6